Fibers and Polymers 2004, Vol.5, No.3, 245-251

Synthesis, Structure, and Thermal Property of Poly(trimethylene terephthalate-*co*-trimethylene 2,6-naphthalate) Copolymers

Young Gyu Jeong, Won Ho Jo*, and Sang Cheol Lee[1]

Hyperstructured Organic Materials Research Center and School of Materials Science and Engineering, Seoul National University, Seoul 151-742, Korea

[1]*School of Advanced Materials and Systems Engineering, Kumoh National University of Technology, Kumi 730-701, Korea*

(Received June 3, 2004; Revised July 21, 2004; Accepted July 28, 2004)

Abstracts: Poly(trimethylene terephthalate-co-trimethylene 2,6-naphthalate)s (P(TT-co-TN)s) with various copolymer composition were synthesized, and their chain structure, thermal property and crystalline structure were investigated by using ^{1}H-NMR spectroscopy, differential scanning calorimetry (DSC) and wide-angle X-ray diffraction (WAXD), respectively. It was found from sequence analysis that all the P(TT-co-TN) copolymers synthesized have a statistical random distribution of TT and TN units. It was also observed from DSC thermograms that the glass transition temperature increases linearly with increasing the TN comonomer content, whereas the melting temperature of copolymer decreases with increasing the corresponding comonomer content in respective PTT- and PTN-based copolymer, showing pseudo-eutectic melting behavior. All the samples melt-crystallized isothermally except for P(TT-co-66 mol % TN) exhibit multiple melting endotherms and clear X-ray diffraction patterns. The multiple melting behavior originates from the dual lamellar population and/or the melting-recrystallization-remelting. The X-ray diffraction patterns are largely divided into two classes depending on the copolymer composition, i.e., PTT and PTN β-form diffraction patterns, without exhibiting cocrystallization.

Keywords: Poly(trimethylene terephthalate), Poly(trimethylene naphthalate), Copolymer, Thermal property, Crystal structure

Introduction

Poly(trimethylene terephthalate) (PTT) and poly(trimethylene 2,6-naphthalate) (PTN) are aromatic polyesters with odd-numbered methylene group in their backbones. The only difference in their chemical structures is that the benzene ring in PTT is replaced by the naphthalene ring in PTN, as shown in Figure 1. Compared to the aromatic polyesters with even-numbered methylene units such as poly(ethylene terephthalate) (PET), poly(ethylene 2,6-naphthalate) (PEN), poly(butylene terephthalate) (PBT), and poly(butylene 2,6-naphthalate) (PBN), PTT and PTN have not attracted much interest from both academia and industry until economical methods for production of 1,3-propandiol and 2,6-naphthalenedicarboxylic acid have been developed. With commercial production of the monomers, PTT and PTN have been recognized as an engineering thermoplastics that can be used for fibers, films, and molding materials.

Numerous studies have been carried out to investigate the crystal structure [1,2], mechanical properties [3-5], crystallization and melting behavior [6-10] of PTT. It was firstly identified by two different groups [1,2] that PTT has a triclinic crystal structure with dimensions of $a = 0.46$, $b = 0.62$, $c = 1.83$ nm, $\alpha = 98°$, $\beta = 90°$, and $\gamma = 112°$. It was also reported by Ward and his coworkers that PTT fiber has better tensile elastic recovery than PET and PBT [3,4]. They showed that this property arises from the chain conformation of PTT backbone in its crystal structure, i.e., the trimethylene unit between terephthalate residues of PTT is in contracted *gauche/gauche* conformation, whereas ethylene unit of PET and butylene unit of PBT are in *trans* and *gauche/trans/gauche* conformation, respectively. In short, the elastic recovery is in the order of PTT > PBT > PET [4]. It has recently been found that the crystallization rate of PTT is faster than that of PET but slower than that of PBT [7] and that PTT exhibits one to three melting endotherms depending on the crystallization temperature, i.e., multiple melting behavior [10]. It has been realized that the multiple melting behavior originates from the dual lamellar population due to the primary and secondary crystallization and/or the melting-recrystallization-remelting [10].

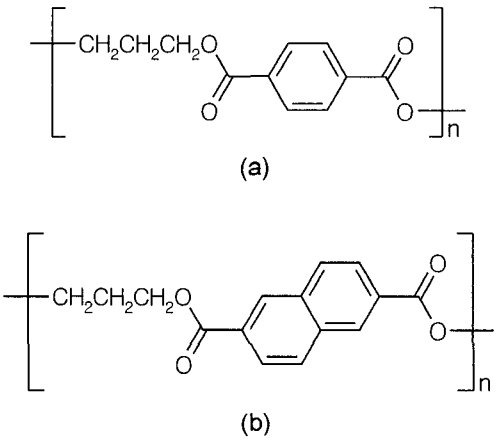

Figure 1. Chemical structures of poly(trimethylene terephthalate) (PTT) and poly(trimethylene 2,6-naphthalate) (PTN).

*Corresponding author: whjpoly@plaza.snu.ac.kr

Polymerization kinetics, thermal properties, and rheological properties of PTN have been intensively studied [11-15]. Recently, crystal structures, crystallization and melting behavior of PTN have been thoroughly investigated by us [16,17]. It was found that, unlike PTT, the PTN has two different crystal structures, α-form and β-form, depending upon the crystallization temperature [16]. The α-form crystal is developed below melt-crystallization temperature of 140 °C, whereas the β-form crystal develops above 160 °C. Both α- and β-form crystals coexist in the sample melt-crystallized isothermally between 140 and 160 °C. However, the relative fraction of α-form crystals decreases with increasing the melt-crystallization temperature from 140 to 160 °C. It was also identified that the PTN β-form is triclinic with dimensions of $a = 0.467$, $b = 0.701$, $c = 2.218$ nm, $\alpha = 100.85$ °, $\beta = 88.78$ °, and $\gamma = 120.63$ ° and that each trimethylene sequence in the crystal lattice takes *gauche/gauche* conformation [17]. This Z-shaped arrangement of chain backbone in the PTN β-form crystal is similar to the chain packing observed in the crystal of PTT. PTN also exhibits multiple melting behavior by showing one to five melting endotherms, depending on the crystallization temperature. It was found that the complex multiple melting behavior is due to a combined mechanism of the existence of different crystal structures of α- and β-forms, the dual lamellar population, and the melting-recrystallization-remelting [16].

Since copolymerization and reactive blending of two or more different polyesters provide a convenient way to prepare the copolyesters with desirable properties through controlling the composition and constitution of copolyesters, studies on copolyesters or reactive blends of two different polyesters have been carried out extensively [18-26]. One of typical examples is poly(trimethylene terephthalate-*co*-trimethylene 2,6-naphthalate) (P(TT-*co*-TN)) copolymers. However, the structure-property relationship of P(TT-*co*-TN) has not been established. In this study, therefore, we synthesized P(TT-*co*-TN)s with various copolymer composition and characterized their chain structure, thermal property, and crystalline structure using ^{1}H-NMR spectroscopy, differential scanning calorimetry (DSC), and wide-angle X-ray diffraction (WAXD). Finally, it is attempted to establish the copolymer composition-structure-property relationship of the copolyester.

Experimental

Synthesis and Characterization of Materials

PTT, PTN, and a series of P(TT-*co*-TN) copolymers were synthesized from 1,3-propanediol (PD), dimethyl terephthalate (DMT), and dimethyl-2,6-naphthalate (DMN) in the melt state using titanium isopropoxide as a catalyst. The catalyst concentration was 2.5×10^{-4} mol/mol diester, where diester indicates DMT and/or DMN. Two-step reaction was performed on a laboratory-scale polymerization reactor with mechanical stirrer. The first-step reaction was the transesterification of DMT and/or DMN with PD. The reaction was carried out at 190 °C under nitrogen atmosphere and the degree of transesterification was monitored by the amount of distilled methanol as the by-product. The second-step was the polycondensation reaction at 260-270 °C under high vacuum condition. At the end of reaction, the product in the melt state was quenched into cold water and then dried under high vacuum condition for several days. The copolymer composition was chosen so that copolymers have 0, 10, 25, 45, 65, 90, and 100 mol % of TN content. The polymers synthesized in this study were used without further purification.

The intrinsic viscosities of all the samples were measured in a dilute solution of phenol and 1,1,2,2-tetrachloroethane (6/4, v/v) mixture at 35 °C using an Ubbelohde viscometer. ^{1}H-NMR spectroscopy was used for determining both the copolymer composition and the degree of randomness of the copolymers. ^{1}H-NMR spectra of the samples in $CDCl_3$/CF_3COOD (5/5, v/v) solutions with tetramethylsilane (TMS) as the internal standard were recorded on a Bruker AMX500 FT-NMR spectrometer operating at 500 MHz.

Melt-quenched amorphous and isothermally melt-crystallized films with 0.4 mm in thickness were prepared by heating the samples to the temperature 30 °C higher than the apparent melting temperature of each sample, holding for 3 min, and then rapidly transferring into cooling water or into another hot plate set at the predetermined crystallization temperature, respectively. The melt-crystallization temperature was chosen to be 30 °C lower than the highest melting temperature (T_{m3}) of each sample (T_{m3} will be discussed later), so that the degree of undercooling for all the samples was 30 °C. The isothermal melt-crystallization was carried out for several or dozens of hours to reach maximum crystallinity at a given temperature.

Thermal Analysis

Thermal properties of the melt-quenched amorphous and the isothermally melt-crystallized samples were measured using a Perkin-Elmer DSC-7 equipped with an intercooler at the heating rate of 20 °C/min. Temperature and heat flow were calibrated using the high-purity indium standard (156.6 °C and 28.45 J/g). The small sample size of 5 ± 0.2 mg was used to minimize the effect of thermal conductivity of polymer. The peaks of melting endotherm and crystallization exotherm for each sample were taken as the apparent melting and crystallization temperature, respectively.

WAXD Analysis

X-ray diffractograms were obtained for the samples melt-crystallized isothermally using a MAC Science M18XHF diffractometer with Ni-filtered Cu-$K\alpha$ radiation ($\lambda = 0.154$ nm, 50 kV, 100 mA) at the scanning rate of 2 °/min. The diffractometer was equipped with a $\theta/2\theta$ goniometer, a divergence slit (1.0 °), a scattering slit (1.0 °), and a receiving slit (0.30 mm). The angular calibration was performed with Si powder ($2\theta = 28.44$ °) standard. The X-ray crystallinity (x) for the samples melt-crystallized isothermally was determined

from X-ray diffraction data in the range of 2θ = 5-40 ° after correction of the Lorentz and polarization factors, using the relation of $x = A_{cr}/(A_{cr} + A_{am})$, where A_{cr} and A_{am} denote the total crystalline and amorphous scattering, respectively.

Results and Discussion

Chain Structure of Materials

A typical ^{1}H-NMR spectrum of P(TT-*co*-TN) copolymer with 44 mol % TN and its peak assignment is presented in Figure 2. Since the peaks corresponding to the protons in naphthalene ring of TN unit are separated into two groups, *d* and *e*, due to magnetically different environment, an equation for determining the copolymer composition from respective peak area can be easily derived as

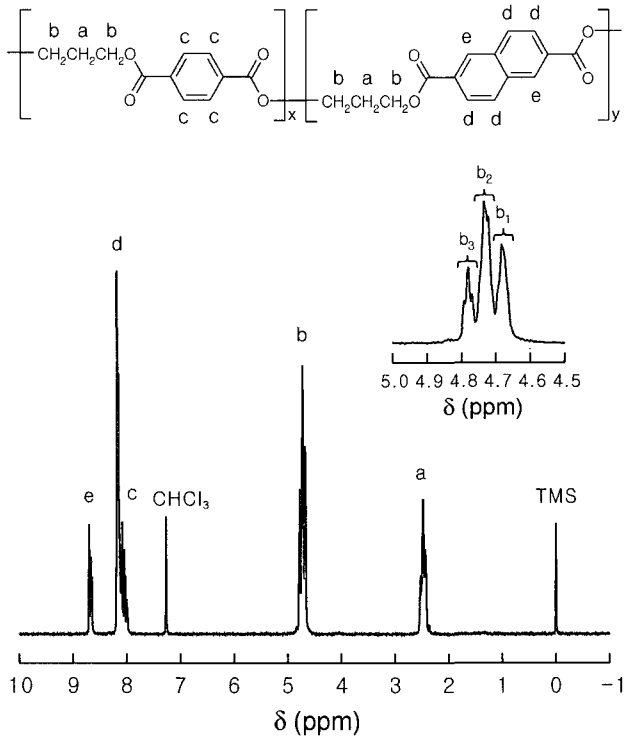

Figure 2. A typical ^{1}H-NMR spectrum of P(TT-*co*-TN) copolymer and its peak assignment.

$$\frac{2a}{e} = \frac{b}{e} = \frac{c+d}{e} = \frac{2(X+Y)}{Y} \quad (1)$$

where *a*, *b*, *c*, *d*, and *e* denote the areas of corresponding peaks in Figure 2, and *X* and *Y* indicate the mole fractions of TT and TN units in copolymer, respectively. When the copolymer composition determined by equation (1) was compared with the feed composition, it was revealed that the copolymer composition is nearly the same as the feed composition, as listed in Table 1. On the other hand, the resonance between 4.5 and 5.0 ppm was used to determine the number-average sequence length and the degree of randomness of the copolymers. An expanded ^{1}H-NMR spectrum in the range of 4.5-5.0 ppm is presented in the inset of Figure 2, where three groups are assigned to TT/TT (b_1), TT/TN or TN/TT (b_2), and TN/TN (b_3) dyads, respectively, in the order of increasing the chemical shift. The relative concentrations of the three dyads are determined from three deconvoluted areas. From the three peak areas ($A_{TT/TT}$, $A_{TT/TN}$, and $AT_{TN/TN}$) corresponding to TT/TT, TT/TN, and TN/TN dyads, the number-average sequence lengths (L_{TT} and L_{TN}) of TT and TN are calculated using the following equations [27,28]:

$$L_{TT} = \frac{2A_{TT/TT} + A_{TN/TT}}{A_{TN/TT}} = \frac{1}{P_{TN/TT}}$$

$$L_{TN} = \frac{2A_{TN/TN} + A_{TT/TN}}{A_{TT/TN}} = \frac{1}{P_{TT/TN}} \quad (2)$$

where $P_{i/j}$ denotes the probability of finding an *i* unit next to a *j* unit in the copolymer chain. When the resulting sequence lengths of TT and TN units are plotted as a function of copolymer composition, as shown in Figure 3, it reveals that both sequence lengths change largely with the copolymer composition. Based on the calculated number-average sequence lengths, the degree of randomness, *DR*, of the copolymers can be defined as [27,28]

Table 1. Composition, intrinsic viscosity, and degree of randomness of polymers

Sample code	Feed composition (mol %)		Copolymer composition[a] (mol %)		Intrinsic viscosity (dl/g)	Degree of randomness (*DR*)
	TT	TN	TT	TN		
PTT	100.0	0.0	100.0	0.0	0.68	
P(TT-*co*-7 mol % TN)	90.0	10.0	92.9	7.1	0.62	1.00
P(TT-*co*-25 mol % TN)	75.0	25.0	74.7	25.3	0.67	1.01
P(TT-*co*-44 mol % TN)	55.0	45.0	56.2	43.8	0.63	1.03
P(TT-*co*-64 mol % TN)	35.0	65.0	36.2	63.8	0.69	1.01
P(TT-*co*-89 mol % TN)	10.0	90.0	11.5	88.5	0.62	1.04
PTN	0.0	100.0	0.0	100.0	0.74	

[a] determined by ^{1}H-NMR.

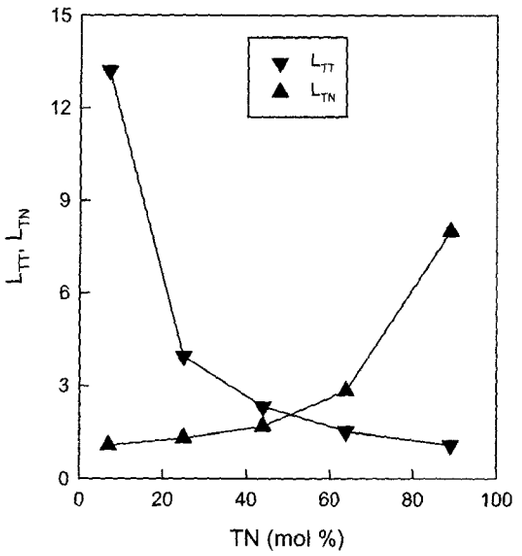

Figure 3. Number-average sequence lengths, L_{TT} and L_{TN}, of TT and TN units as a function of copolymer composition.

$$DR = P_{TN/TT} + P_{TT/TN} = 1/L_{TT} + 1/L_{TN} \quad (3)$$

By definition, $DR = 0$ is for a homopolymer mixture or virtually for diblock copolymer, $DR = 1$ for a random copolymer, indicating that the distribution of comonomer units obeys the Bernoullian statistics, and DR = 2 for an alternating copolymer, e.g., a chain consisting of only TT/TN dyads. As can be seen in Table 1, the *DR* values of P(TT-*co*-TN) copolymers are nearly unity, which indicates that all the P(TT-*co*-TN) copolymers synthesized in this study are statistically random copolymers.

The intrinsic viscosities of all the samples were in the range of 0.62-0.74 dl/g, as listed in Table 1, indicating that all the samples synthesized have relatively high molecular weight to form in film or fiber.

Thermal Property and Crystalline Structure

Figure 4 shows heating thermograms of the melt-quenched amorphous PTT, PTN, and P(TT-*co*-TN) copolymers. Among them, three samples, PTT, P(TT-*co*-7 mol % TN), and P(TT-*co*-25 mol % TN), exhibit clearly cold-crystallization and melting. The cold-crystallization exotherm shifts to higher temperature and becomes broader with increasing the TN comonomer content, whereas the melting endotherm shifts to lower temperature and becomes broader, as shown in Figures 4 and 5. This is probably because the crystal becomes thinner and less perfect due to the decrease of the sequence length of crystallizable TT units, as the TN content in copolymer increases. On the other hand, PTN shows a very small melting endotherm, as can be seen in Figure 4(g). When PTN is melt-crystallized dynamically at various cooling rates, the enthalpy relaxation peak accompanying with the glass transition becomes larger with decreasing the cooling rate, while melting endotherms

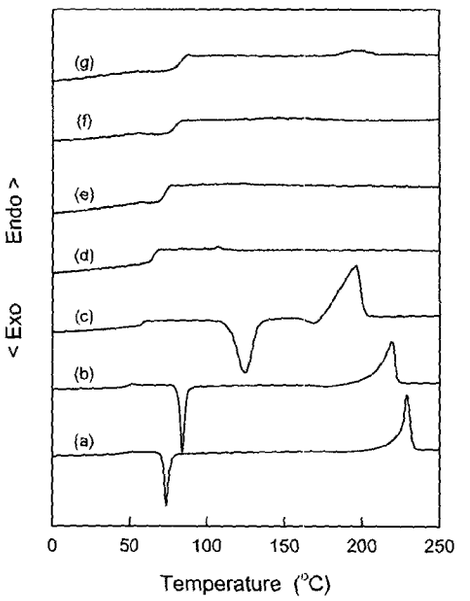

Figure 4. DSC heating thermograms of the melt-quenched amorphous samples: (a) PTT, (b) P(TT-*co*-7 mol % TN), (c) P(TT-*co*-25 mol % TN), (d) P(TT-*co*-44 mol % TN), (e) P(TT-*co*-64 mol % TN), (f) P(TT-*co*-89 mol % TN), (g) PTN.

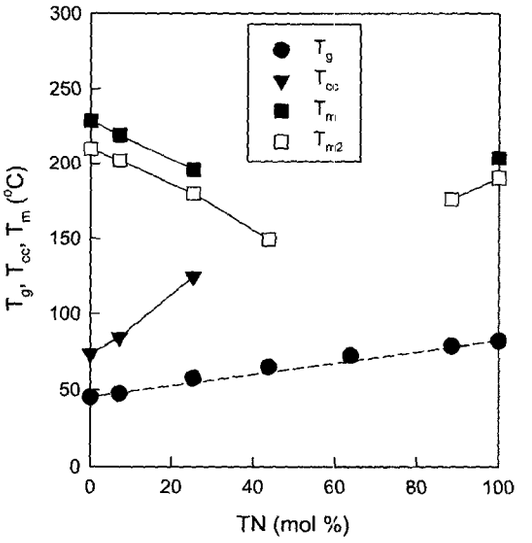

Figure 5. Glass transition (T_g), cold-crystallization (T_{cc}), and melting (T_m) temperatures of P(TT-*co*-TN) copolymers as a function of copolymer composition. The filled symbols are for the melt-quenched amorphous samples and the open symbols for the samples melt-crystallized isothermally under the degree of under-cooling of 30 °C. The broken line is based on the Gibbs-DiMarzio theory for glass transition temperature of random copolymer.

of samples crystallized dynamically at the cooling rates of 2, 20, and 200 °C/min are small except the case of 1 °C/min, as shown in Figure 6. A sharp melting endotherm of the sample

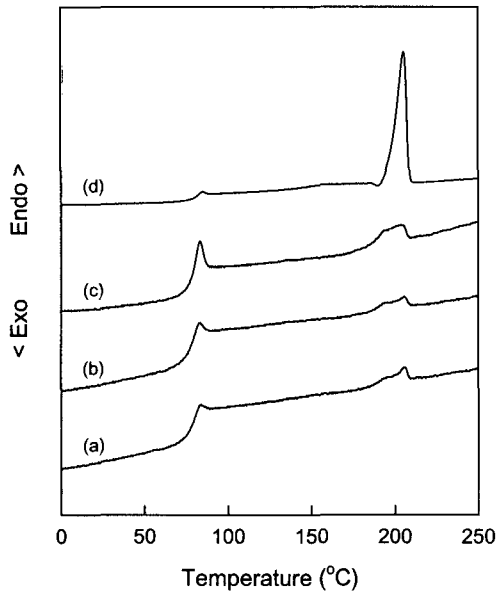

Figure 6. DSC heating thermograms of the PTN samples melt-crystallized dynamically at various cooling rates: (a) 200 °C/min, (b) 20 °C/min, (c) 2 °C/min, (d) 1 °C/min.

crystallized dynamically at the cooling rate of 1 °C/min is observed at 207 °C. This melting behavior of PTN depending on the cooling rate indicates that the crystallization rate of PTN is very slow. Consequently, the melt-quenched amorphous PTN and its copolymers with above 44 mol % TN do not show clear cold-crystallization and melting at the heating rate of 20 °C/min, as shown in Figure 4. It was found by us that the relative crystallization rate is in the order of PBN > PEN >> PTN [29]. When the glass transition temperature of P(TT-*co*-TN) copolymer is plotted against the TN comonomer content, it increases linearly with increasing the TN comonomer content, as shown in Figure 5. The broken line in Figure 5 is based on the Gibbs-DiMarzio theory which is applied to calculation of the glass transition temperatures of amorphous random copolymers [30,31]. The equation is given by

$$T_g = X_A T_{g_A} + X_B T_{g_B} \quad (4)$$

where X_A and X_B are the mole fractions of monomer units A and B, respectively. This equation is identical in form to an empirical equation of Wood [32], which is widely used for the glass transition temperature of random copolymers.

X-ray diffraction patterns for the samples melt-crystallized isothermally under the degree of undercooling of 30 °C are shown in Figure 7. All the samples except for P(TT-*co*-64 mol % TN) show clear diffraction patterns. PTT and P(TT-*co*-TN) copolymers with 7, 25, and 44 mol % TN exhibit the typical diffraction pattern of PTT, while PTN and P(TT-*co*-89 mol % TN) display the diffraction pattern of PTN β-form. With increasing the corresponding comonomer content in respective PTT- or PTN-based copolymers, the X-ray crystallinity

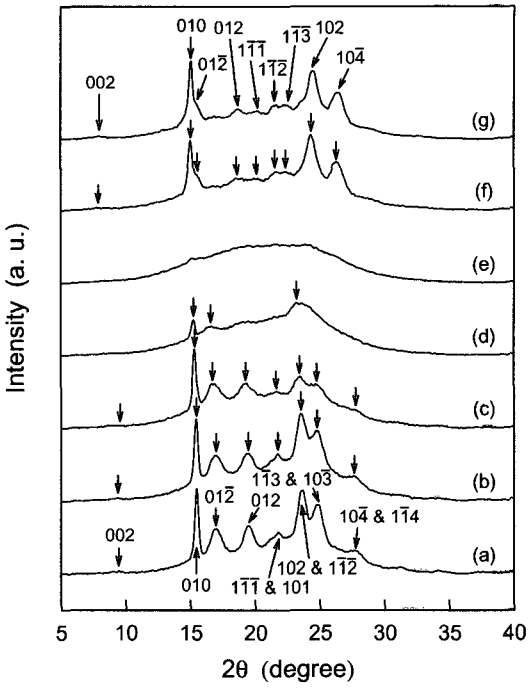

Figure 7. WAXD patterns of the samples melt-crystallized isothermally under the degree of undercooling of 30 °C: (a) PTT, (b) P(TT-*co*-7 mol % TN), (c) P(TT-*co*-25 mol % TN), (d) P(TT-*co*-44 mol % TN), (e) P(TT-*co*-64 mol % TN), (f) P(TT-*co*-89 mol % TN), (g) PTN.

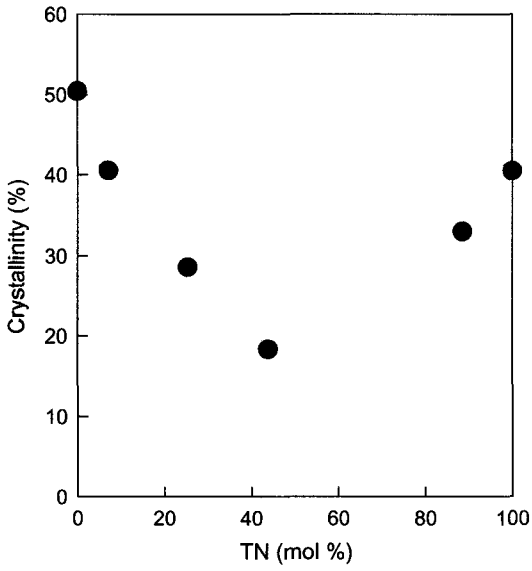

Figure 8. X-ray crystallinity as a function of copolymer composition. The crystallinity was calculated using WAXD patterns shown in Figure 7.

of copolymers is decreased (Figure 8) but the diffraction peak positions remain nearly unchanged (Figure 7). It indicates that P(TT-*co*-TN) copolymers do not cocrystallize due to the imcompatibility of two components in each crystal lattice,

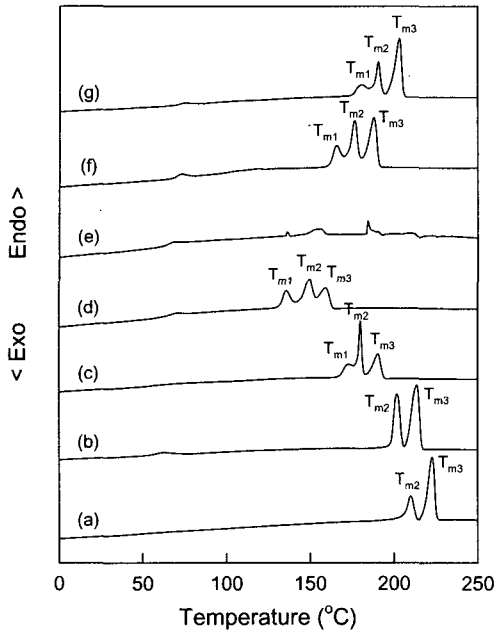

Figure 9. DSC heating thermograms of the samples melt-crystallized isothermally under the degree of undercooling of 30 °C: (a) PTT, (b) P(TT-*co*-7 mol % TN), (c) P(TT-*co*-25 mol % TN), (d) P(TT-*co*-44 mol % TN), (e) P(TT-*co*-64 mol % TN), (f) P(TT-*co*-89 mol % TN), (g) PTN.

although PTT and PTN have a similar crystal structure and chain conformation as noted in the introduction section.

Figure 9 shows heating thermograms of the samples melt-crystallized isothermally under the same degree of undercooling of 30 °C. PTT, PTN, and their copolymers except for P(TT-*co*-64 mol % TN) exhibit two or three melting endotherms, i.e., multiple melting behavior, depending upon both the copolymer composition and the melt-crystallization temperature. Even though the origin of multiple melting behavior has still been debated, three mechanisms for multiple melting behavior have been generally accepted, namely, (i) the existence of different crystal structures [33-36] (ii) the dual lamellar population model due to the primary and secondary crystallization [37-40] and (iii) the melting-recrystallization-remelting model [41-44]. The multiple melting behavior due to the existence of different crystal structures has been proposed for syndiotactic polystyrene [33,34], isotactic polypropylene [35] and poly(vinylidene fluoride) [36]. In the dual lamellar population model, primary lamellar crystals are first formed in thicker crystalline lamellae, and secondary lamellar crystals are then formed in between the primary lamellar crystals, so that the primary lamellar crystals have higher melting temperature than the secondary lamellar crystals [37-40]. In the melting-recrystallization-remelting model, the lamellar crystals present initially melt, the melted lamellar crystals undergo a continuous process of recrystallization yielding thicker lamellar crystals, and then the recrystallized crystals melt at higher temperatures [41-44]. In this study, since all the samples melt-crystallized isothermally under the same degree of undercooling of 30 °C exhibit the typical diffraction pattern of PTT or PTN β-form, depending on the copolymer composition, it can be concluded that the multiple melting behavior shown in Figure 9 arises from the dual lamellar population and/or the melting-crystallization-remelting. According to the references 7 and 16 on multiple melting behavior of PTT and PTN, therefore, the melting endotherms shown in Figure 9 can be assigned as follows: T_{m1} is due to melting of crystals formed during secondary crystallization, T_{m2} due to melting of crystals developed during the primary crystallization, and T_{m3} due to melting of crystals recrystallized after melting of the primary crystals. It is well known that T_{m1} and T_{m2} except for T_{m3} are dependent on the crystallization temperature [7,16]. When the melting temperature (T_{m2}) due to the primary crystal is plotted as a function of the TN comonomer content, as can be seen in Figure 5, it shows pseudo-eutectic melting behavior, since P(TT-*co*-66 mol % TN) around the expected eutectic composition does not show a clear melting endotherm, as shown in Figure 9(e), which is consistent with the X-ray diffraction result.

Conclusions

Chain structure, thermal property, and crystalline structure of P(TT-*co*-TN) copolymers with various copolymer composition were investigated by using ^{1}H-NMR, DSC, and WAXD, respectively. From sequence analysis, all the P(TT-*co*-TN)s synthesized in this study are found to be statistically random copolymers. It was also observed from DSC thermograms that the glass transition temperature increases linearly from 45 to 82 °C with increasing the TN comonomer content in the copolymer, while the melting temperature decreases with increasing the corresponding comonomer content in respective PTT- or PTN-based copolymer, showing the pseudo-eutectic melting behavior. All the samples melt-crystallized isothermally except for P(TT-*co*-66 mol % TN) exhibit clear multiple melting endotherms and X-ray diffraction patterns. The multiple melting behavior arises from the dual lamellar population and/or the melting-recrystallization-remelting. The X-ray diffraction patterns are largely divided into two classes depending on the copolymer composition, i.e., PTT and PTN β-form diffraction patterns. However, the X-ray crystallinity of copolymers decreases with increasing the corresponding comonomer content in respective PTT- or PTN-based copolymers, while the diffraction peak positions remain nearly unchanged, indicating that the copolymers do not cocrystallize due to the incompatibility of two components in each crystal structure.

Acknowledgement

The authors thank the Korea Science and Engineering Foun-

dation for financial support through the Hyperstructured Organic Materials Research Center.

References

1. S. Poulin-Dandurand, S. Pérez, J. F. Revol, and F. Brisse, *Polymer*, **20**, 419 (1979).
2. I. J. Desborough, I. H. Hall, and J. A. Neisser, *Polymer*, **20**, 545 (1979).
3. E. Jakeways, I. M. Ward, M. A. Wilding, I. H. Hall, I. J. Desborough, and M. G. Pass, *J. Polym. Sci., Polym. Phys.*, **13**, 799 (1975).
4. I. M. Ward and M. A. Wilding, *J. Polym. Sci., Polym. Phys.*, **14**, 263 (1976).
5. E. E. Shafee, *Polymer*, **44**, 3727 (2003).
6. M. Pyda and B. Wunderlich, *J. Polym. Sci., Polym. Phys.*, **38**, 622 (2000).
7. J.-M. Huang and F.-C. Chang, *J. Polym. Sci., Polym. Phys.*, **38**, 934 (2000).
8. P.-D. Hong, W.-T. Chung, and C.-F. Hsu, *Polymer*, **43**, 3335 (2002).
9. M. Chen, C. C. Chen, K. Z. Kz, and R. M. Ho, *J. Macromol. Sci., Phys.*, **B41**, 1063 (2002).
10. P.-L. Wu and E. M. Woo, *J. Polym. Sci., Polym. Phys.*, **41**, 80 (2003).
11. R. S. Tsai and Y. D. Lee, *J. Polym. Res.*, **5**, 77 (1998).
12. S. K. Hwang, C. Yeh, L. S. Chen, T. F. Way, L. M. Tsay, K. K. Liu, and L. T. Chen, *Polymer Preprints*, **40**, 611 (1999).
13. U. Stier, F. Gahr, and W. Oppermann, *J. Appl. Polym. Sci.*, **80**, 2039 (2001).
14. U. Stier and W. Oppermann, *J. Polym. Sci., Polym. Phys.*, **39**, 620 (2001).
15. U. Stier, D. Schawaller, and W. Oppermann, *Polymer*, **42**, 8753 (2001).
16. Y. G. Jeong, W. H. Jo, and S. C. Lee, *Polymer*, **44**, 3259 (2003).
17. Y. G. Jeong, W. H. Jo, and S. C. Lee, *Polymer*, **45**, 379 (2004).
18. C. Hwo, T. Forschner, R. Lowtan, D. Gwyn, and B. Cristea, *J. Plast. Film Sheet*, **15**, 219 (1999).
19. X. S. Wang, X. G. Li, and D. Y. Yan, *J. Appl. Polym. Sci.*, **78**, 2025 (2000).
20. J. M. Huang and F. C. Chang, *J. Appl. Polym. Sci.*, **84**, 850 (2002).
21. T. W. Son, K. I. Kim, N. H. Kim, M. G. Jeong, and Y. H. Kim, *Fiber Polym.*, **4**, 20 (2003).
22. E. M. Woo and L. T. Lee, *Polym. Bull.*, **50**, 33 (2003).
23. C. P. Roupakias, G. Z. Papageorgiou, and G. P. Karayannidis, *J. Macromol. Sci. Pure & Appl. Chem.*, **A40**, 791 (2003).
24. F. C. Chiu, K. H. Huang, and J. C. Yang, *J. Polym. Sci., Polym. Phys.*, **41**, 2264 (2003).
25. E. M. Woo and Y. H. Kuo, *J. Polym. Sci., Polym. Phys.*, **41**, 2394 (2003).
26. J. H. Kim, J. H. Park, H. K. Jang, J. Y. Yoon, and W. S. Lyoo, *J. Appl. Polym. Sci.*, **90**, 2200 (2003).
27. R. Yamadera and M. Murano, *J. Polym. Sci., Polym. Chem.*, **5**, 2259 (1967).
28. J. L. Koenig, "Chemical Microstructure of Polymer Chains", John Wiley and Sons, New York, 1980.
29. Y. G. Jeong, Ph.D. Thesis, Seoul National University, Seoul, Korea, 2003.
30. J. H. Gibbs and E. A. DiMarzio, *J. Chem. Phys.*, **28**, 373 (1958).
31. E. A. DiMarzio and J. H. Gibbs, *J. Polym. Sci.*, **40**, 121 (1959).
32. L. A. Wood, *J. Polym. Sci.*, **28**, 319 (1958).
33. Y. S. Sun and E. M. Woo, *Macromolecules*, **32**, 7836 (1999).
34. R. H. Lin and E. M. Woo, *Polymer*, **41**, 121 (2000).
35. R. J. Samuels, *J. Polym. Sci., Polym. Phys.*, **13**, 1417 (1975).
36. W. M. Prest, Jr. and D. J. Luca, *J. Appl. Phys.*, **46**, 4136 (1975).
37. K. N. Kruger and H. G. Zachmann, *Macromolecules*, **26**, 5202 (1993).
38. R. K. Verma and B. S. Hsiao, *Trends Polym. Sci.*, **4**, 312 (1996).
39. R. K. Verma, H. Marand, and B. Hsiao, *Macromolecules*, **29**, 7767 (1996).
40. Z. Denchez, A. Nogales, T. A. Ezquerra, J. Fernandes-Nascimento, and F. J. Balta-Calleja, *J. Polym. Sci., Polym. Phys.*, **38**, 1167 (2000).
41. G. Groeninckx and H. Reynaers, *J. Polym. Sci., Polym. Phys.*, **18**, 1325 (1980).
42. D. J. Blundell and B. N. Osborn, *Polymer*, **24**, 953 (1983).
43. Y. Lee and R. S. Porter, *Macromolecules*, **20**, 1336 (1987).
44. A. Jonas and R. Legas, *Macromolecules*, **26**, 813 (1993).